THE JOURNAL OF BIOLOGICAL CHEMISTRY VOL. 289, NO. 1, pp. 299–311, January 3, 2014

Mitogen-activated Protein Kinase-mediated Licensing of Interferon Regulatory Factor 3/7 Reinforces the Cell Response to Virus*

Received for publication, September 19, 2013, and in revised form, November 22, 2013 Published, JBC Papers in Press, November 25, 2013, DOI 10.1074/jbc.M113.519934

Sonja Schmid[‡], **David Sachs**[§], **and Benjamin R. tenOever**[‡1]

From the Departments of [‡]*Microbiology and* [§]*Genomics, Icahn School of Medicine at Mount Sinai, New York, New York 10029*

Background: Virus infections of mammals have a wide spectrum of outcomes, ranging from immediate clearance to severe disease.
Results: MAP3K8-mediated phosphorylation of IRF3 promotes IRF3:IRF7 dimer formation and strengthens the antiviral response.
Conclusion: The MAP3K8/IRF7 signaling axis ensures that the intracellular innate immune response correlates to the degree of virus threat.
Significance: Understanding the intrinsic cellular response to viruses provides insight into the underlying causes of virus pathogenicity.

The induction of the intrinsic antiviral defense in mammals relies on the accumulation of foreign genetic material. As such, complete engagement of this response is limited to replication-competent viruses. Interferon regulatory factors (IRFs) are mediators of this defense with shared enhancer elements but display a spectrum of transcriptional potential. Here we describe a mechanism designed to enhance this response should a pathogen not be successfully inhibited. We find that activation of IRF7 results in the induction of MAP3K8 and restructuring of the antiviral transcriptome. MAP3K8 mediates the phosphorylation and repression of IRF3 homodimers to promote greater transcriptional activity through utilization of IRF3:IRF7 heterodimers. Among the genes influenced by the MAP3K8/IRF7 signaling axis are members of the SP100 gene family that serve as general transcriptional enhancers of the antiviral defense. We propose that this feed forward loop serves to reinforce the cellular response and is reserved for imminent threats to the host.

The cellular defense to virus in mammals consists of multiple signaling events and requires a myriad of protein components. Upon productive viral infection, pathogen-associated molecular patterns (PAMPs)[2] are recognized by cellular receptors and trigger a powerful signaling cascade aimed at clearing the microbe (1). Viral PAMPs, including double-stranded RNA, bind pattern recognition receptors such as Toll- and RIG-I-like receptors (2, 3). Pattern recognition receptor activation results in the assembly of a signaling complex at the mitochondrial membrane that includes MAVS (also known as IPS-I, Cardif, and VISA) and engagement of both the classical IKK and IKK-related kinases as well as MAPKs, culminating in NFκB, interferon regulatory factor (IRF), and AP1 activation, respectively (4). This coordinated activation of transcription factors leads to formation of an enhanceosome in the promoter of the primary type I interferon (IFN-I) gene product, IFNβ (5). Transcriptional induction of the IFNβ gene results in rapid secretion of this antiviral cytokine, which functions in both autocrine and paracrine manners. IFNβ engagement with its receptor results in a second signal transduction event that includes the assembly of kinases, resulting in a multisubunit transcription complex termed the IFN-stimulated gene factor 3 (ISGF3) (6). ISGF3 binds to IFN-stimulated response elements (ISREs) in the promoters of hundreds of IFN-stimulated genes (ISGs), whose expression confers an antiviral state to the cell (6–8). The products of ISGs collectively function to inhibit virus replication. This is achieved by blocking many essential cellular functions required for virus propagation. However, it is noteworthy that although IFN-I signaling primes cells to engage in this aggressive defense, they too require a critical threshold of PAMP before functioning (9, 10). Such a dynamic ensures that the cell does not unnecessarily shut down cellular processes that are essential for the host, as well as the pathogen. Should PAMP levels never reach the critical mass necessary to activate the primed antiviral response, a number of phosphatases are also induced that serve to reset the cell defenses back to base line (11).

The main effectors that both initiate and amplify the antiviral response of the cell are a family of transcription factors called interferon regulatory factors (IRFs) (12). With nine members, IRFs have been implicated in a diverse breadth of cellular activities with IRF1, IRF2, IRF3, IRF5, IRF7, and IRF9 being directly

* This work was supported, in whole or in part, by National Institutes of Health Grant A1080624 from the NIAID.
[1] To whom correspondence should be addressed. Tel.: 212-241-7849; Fax: 212-534-1684; E-mail: benjamin.tenoever@mssm.edu.
[2] The abbreviations used are: PAMP, pathogen-associated molecular patterns; IRF, interferon regulatory factor; ISG, IFN-stimulated gene; ISGF3, ISG factor 3; ISRE, IFN-stimulated response element; IRF-E, IRF binding element; VSV, vesicular stomatitis virus; pen/strep, penicillin/streptomycin; MOI, multiplicity of infection; hpi, hour(s) post-infection; hpt, hours post-transfection; LUC, luciferase; IP, immunoprecipitation; CIP, calf intestinal alkaline phosphatase; WCE, whole cell extract; WB, Western blot; qPCR, quantitative PCR; mRNA-seq, mRNA deep sequencing; coIP, co-immunoprecipitation; PML-NBs, promyeolytic leukemia nuclear bodies.

implicated in some aspect of the antiviral response (8, 13–19). Among these, IRF3 and IRF7 are particularly noteworthy, because these factors have been directly implicated in the transcriptional induction of IFNβ as well as having the capacity to induce ISGs in an IFN-I-independent manner (20–23). Crystal structure and promoter analysis identified the consensus binding sequence for the IRF family, the so-called IRF binding element (IRF-E) (24, 25). However, each IRF family member displays subtle differences in their binding specificities within the broad IRF consensus sequence and thereby performs a distinct function in cellular processes (26–30). For example, the capacity of IRF3 to bind to an IRF-E demands an 8-nucleotide consensus in which loss of a single base renders the site unrecognizable. In contrast, IRF7 can engage an IRF-E that has up to three bases that do not conform to the consensus (20, 31). This dynamic limits the transcriptional output of IRF3 to only a handful of genes, whereas IRF7 is commonly referred to as the "master regulator" of the antiviral response (23, 32).

Another unique attribute of IRF7 is that, as a result of its unique binding properties, it can also induce many genes that were once thought to be strictly ISGs (20, 33). In comparing the IRF7-dependent transcriptome to the response to IFN-I, we identified a very small subset of genes that were unique to IRF7; one such gene was MAP3K8 (COT, TPL2) (20). MAP3K8 signaling serves important functions in innate and adaptive immunity as well as in cancer as a potential proto-oncogene (34). How MAP3K8 is activated and performs its function remains unclear. Studies show that MAP3K8 binds the p50 (NFκB1) precursor p105 under steady state conditions, which blocks its activation and its proteasomal degradation (35, 36). Stimuli, such as ligands of Toll-like receptors or the TNF receptor superfamily, which activate IKKα/β also lead to proteolysis of p105, release MAP3K8 and allow its activation by as yet unknown kinases (37–39). Active MAP3K8 directly phosphorylates the MAP2K MEK, which then activates the MAPK ERK (39, 40). Besides this main function, MAP3K8 is also implicated in the activation of MAPK8 (JNK), MAPK14 (p38), and the transcription factors NFAT and NFκB (37, 41–43). Genes that are transcriptionally or post-transcriptionally regulated via MAP3K8 include pro-inflammatory cytokines and secondary mediators, as well as anti-inflammatory cytokines (38–40, 44–48). Surprisingly, the role of MAP3K8 in innate immunity has been limited to models of bacterial infection, and extensive studies using viral pathogens are lacking.

Given our previous studies showing the robust induction of MAP3K8 by IRF7, we hypothesized that this kinase may have a relevant role in the antiviral response. Here we show that MAP3K8 is induced and activated during a viral infection in an IRF7-dependent manner and that active MAP3K8 inhibits the transcriptional activity of IRF3 while simultaneously promoting the formation of IRF3:IRF7 dimers and activating the ERK pathway. Lack of MAP3K8 leads to alterations in the antiviral transcriptome, which ultimately increase the vulnerability of the cell to viruses. Three members of the SP100 gene family, SP100, SP110, and SP140, are among the genes that show the highest dependence on the IRF7/MAP3K8 axis for transcriptional induction. We show that SP100 increases IFNβ expression during infection, which partially explains increased viral replication in cells deficient in MAP3K8. This finding provides a molecular mechanism for the amplification of the antiviral response of the cell and establishes a framework for how it is maintained at a level that is proportional to the pathogenic threat that initiated it.

EXPERIMENTAL PROCEDURES

Viruses—Recombinant wild-type vesicular stomatitis virus (VSV) and VSV harboring a methionine to arginine substitution at amino acid position 51 of the VSV matrix protein (VSV-M51R) were previously described (49). The attenuated recombinant influenza A virus strain harboring two amino acid substitutions in NS1 (PR/8/34 NS1-R38A/K41A) was previously described (50).

Cell Culture and Reagents—HEK293T, 2FTGH cells, and murine fibroblasts were cultured in DMEM (Invitrogen) supplemented with 10% FBS and 1× penicillin/streptomycin (pen/strep). HEK293T cells stably expressing human IRF7 were generated using a lentiviral vector encoding IRF7 as previously described (20). *Map3k8*$^{+/+}$ and *Map3k8*$^{-/-}$ fibroblasts were a kind gift of Dr. Philip N. Tsichlis (Thomas Jefferson University, Philadelphia, PA). Transfection of DNA was performed with Lipofectamine 2000 (Invitrogen). siRNAs against human MAP3K8 (Santa Cruz; catalog no. 35095) and control siRNAs (Santa Cruz; catalog no. 37007) were transfected at a final concentration of 40 nM in Opti-MEM I reduced serum medium (Invitrogen), using Lipofectamine RNAiMAX (Invitrogen) according to the manufacturers' instructions. Infection of cells with PR/8/34 NS1-R38A/K41A was performed at a multiplicity of infection (MOI) of 3 in complete medium. Infection of cells with VSV was performed at the indicated MOI in DMEM supplemented with 1% pen/strep. 1 h post-infection (hpi), cells were washed twice with PBS and subsequently cultured in DMEM, 10% FBS, 1× pen/strep.

Plasmids—Expression plasmids for FLAG-tagged human IRF3, IRF7, IRF9, STAT1, STAT2, TBK1, IKKϵ, N-terminal RIG-I (RIG-IN), and MAVS, as well as HA-tagged IRF3, IRF7, MDA5, and MAVS, were previously described (20, 51, 52). The human MAP3K8 ORF was amplified from cDNA with the following primers: forward, 5′-ATGGAGTACATGAGCACTGG-3′; and reverse, 5′-TCAGCCATATTCAAGCGTTGG-3′. The PCR product was first cloned into TOPO (Invitrogen) and then moved either via BamHI/BglII and XbaI or via SacI and XhoI into pFLAG-CMV2 (Sigma) or pCAGGS (53), respectively. To generate truncation and point mutants of FLAG-IRF3, the IRF3 ORF was first cloned into TOPO. Site-directed mutagenesis was performed to introduce STOP codons or alanine substitutions with the QuikChange site-directed mutagenesis kit (Stratagene) according to the manufacturer's instructions. The mutated IRF3 ORF was then moved into pCAGGS-FLAG via NotI and XhoI, using the In-Fusion HD cloning system (Clontech). The reporter constructs encoding firefly luciferase (LUC) under control of PRD(III-I) of the IFNβ promoter or the ISG15-ISRE were previously described (20). The vector expressing LUC under the control of the human *MAP3K8* promoter contains nucleotides −915 to +178 (0 corresponds to the transcriptional start site of *MAP3K8* mRNA) in the multiple cloning site of pLUC-MCS (Stratagene). The following primers were used to amplify the

promoter region from genomic DNA: forward, 5′-TGGCGGGGCATTGGGAATGT-3′; and reverse, 5′-AGCGGAGCGGACGAGTGAGA-3′. The PCR product was first cloned into TOPO and then moved via BamHI and XhoI into pLUC-MCS. To generate a stable cell line expressing human IRF7, a lentiviral vector previously described was used (20). Plasmids encoding for EYFP fused human SP100B and SP100C were a kind gift from Dr. Susan M. Janicki (Wistar Institute, Philadelphia, PA) and were previously described (54).

Luciferase Assay—5×10^5 293T cells were transfected with 100 ng/expression plasmid together with 200 ng of the indicated pLUC-construct and 10 ng of a construct constitutively expressing *Renilla* luciferase (pRL-TK; Promega) to normalize for transfection efficiency. When increasing amounts of MAP3K8 were added to the assay, 0.8, 3, 12, 50, or 200 ng of the FLAG-MAP3K8 expressing plasmid were used. Empty vector served to fill up each transfection reaction to 800 ng of total plasmid. LUC activity was determined 24 hpt using a dual-luciferase reporter assay system (Promega).

Electrophoretic Mobility Shift Assay—2×10^6 HEK293T cells were transfected with 1 μg/expression plasmid, and empty vector served to fill up each transfection reaction to 4 μg of total plasmid. As indicated, 14 hpt medium was changed, and 30 IU/ml of IFNβ (BEI Resources) was added. Whole cell extracts were obtained 24 hpt, and EMSAs were performed as described previously (55).

In Vivo Labeling—8×10^5 HEK293T cells were transfected on 12-well plates with 0.8 μg/expression plasmid, and empty vector served to fill up each transfection reaction to 1.6 μg of total plasmid. Each transfection reaction was done in duplicate. 20 hpt, one set of transfections was incubated for 4 h with 750 μl of labeling medium (DMEM without sodium phosphate and sodium pyrovate (Invitrogen), 1% FBS, 1× pen/strep, and 5 μl of [γ-^{32}P]ATP (10 mCi/ml; PerkinElmer Life Sciences)) per well. The other set of transfections was incubated with DMEM, 1% FBS, and 1× pen/strep. 24 hpt, immunoprecipitation was performed as described below.

Immunoprecipitation (IP) and Calf Intestinal Alkaline Phosphatase (CIP) Treatment—5×10^6 HEK293T cells were transfected with 2 μg/expression plasmid, and empty vector served to fill up each transfection reaction to 8 μg of total plasmid. 24 hpt, cells were washed once with PBS and subsequently lysed with 750 μl of lysis buffer (1% Nonidet P-40, 5 mM EDTA, 10% glycerol, 30 mM NaF, 50 mM Tris), supplemented with 1 mM PMSF and 1× complete EDTA-free protease inhibitor mixture (Roche Applied Science) to prepare whole cell extract (WCE). 650 μl of WCE were incubated with 4 μl of either anti-HA (HA7; Sigma) or anti-FLAG (M2; Sigma) antibody or with 2 μg of anti-CBP (A22; Santa Cruz) antibody overnight at 4 °C. Next day 50 μl of 50:50 slurry of protein G-agarose beads (Roche Applied Science) were added and incubated for 1 h at 4 °C. Afterward the beads were washed four times with 500 μl of lysis buffer, 5 min each. In the case of IP with anti-HA and anti-CBP, beads were resuspended in 50 μl of standard SDS loading dye and analyzed by WB. In the case of IP with anti-FLAG, bound protein was eluted twice with 300 μg/ml of FLAG peptide (F3290; Sigma) for 20 min each. Eluate was either directly used for WB analysis or treated with CIP to remove phosphorylation. For CIP treatment, half of the eluate was incubated with 5 μl of CIP (M0290; New England Biolabs) in 1× NEBuffer 3 for 1 h at 37 °C. The other half was treated identically, except CIP was replaced with double distilled H_2O. Subsequently, protein was analyzed by WB.

Western Blot Analysis—WB analysis was performed as previously described (56). Antibodies specific to IRF3 (FL425; Santa Cruz), IRF7 (G8; Santa Cruz), CBP (A22; Santa Cruz), and MAP3K8 (M20; Santa Cruz) were used at a 1:200 dilution; antibodies specific to ACTIN (ACTN05; Thermo Scientific), FLAG (M2; Sigma), HA (HA7; Sigma), IAV-NP (NR4544; BEI Resources), and VSV-G (A00199; GenScript) were used at a 1:1,000 dilution; and antibodies specific to P-ERK1/2 (D13.14.4E; Cell Signaling) and ERK1/2 (3A7; Cell Signaling) were used at a 1:2,000 dilution.

Immunofluorescence Analysis—Cells were fixed on glass coverslips with 4% formaldehyde in PBS for 10 min and subsequently permeabilized with 0.5% Nonidet P-40 in PBS for 10 min. After two washes with PBS, cells were blocked with 5% BSA in PBS for 30 min. Cells were incubated with the antibody specific to FLAG (M2; Sigma) for 2 h at a 1:500 concentration in 1% BSA. After three washes with PBS, cells were incubated with secondary antibody labeled with Rhodamine Red (Jackson ImmunoResearch) at 1:750 in 1% BSA for 1 h. Afterward, nuclei were stained with Hoechst 33342 dye (Invitrogen) for 15 min at a 1:50,000 dilution in PBS. Following four washes, coverslips were mounted on glass slides with Prolong Gold Antifade (Invitrogen). Images were captured with the Zeiss Axioplan 2 microscope.

Quantitative PCR (qPCR)—qPCR was performed as previously described (56).

mRNA Deep Sequencing (mRNA-seq)—For mRNA-seq, RNA from duplicate experiments of VSV-M51R-infected *Map3k8*$^{+/+}$ and *Map3k8*$^{-/-}$ fibroblasts was analyzed. mRNA-seq was done as previously described (57). Briefly, mRNA was isolated from 1 μg of RNA using sera oligo(dT) beads. Isolated RNA was used for cDNA synthesis with SuperScript II reverse transcriptase (Invitrogen). Samples then underwent second strand synthesis, end repair, A-tailing, ligation, and PCR using the Illumina Truseq kit (Illumina; catalog no. 1502062). The quality of amplified cDNA library was tested using the Bioanalyzer DNA 1000 assay. mRNA-seq libraries were clustered with cBOT (Illumina) and then run on HiSeq (Illumina) for 100-base single read sequencing. Reads were analyzed using a pipeline based on Bowtie and Samtools and aligned to the murine open reading frame database available from Ensembl Biomart. Individual genes were normalized as a percentage of total sample reads mapping to the reference genome.

RESULTS

MAP3K8 Is Transcriptionally Induced and Activated upon Viral Infection—We previously identified MAP3K8 as an IRF7-induced gene, through comparison of the IRF3-, IRF7-, and ISGF3-mediated transcriptomes (20). Given the specific nature of MAP3K8 induction by IRF7, we examined the transcriptional regulation of this kinase by standard firefly LUC assays under the control of the human *MAP3K8* promoter. In agreement with our published results, only activated IRF7, and not IRF3 or the components of the ISGF3 complex (STAT1,

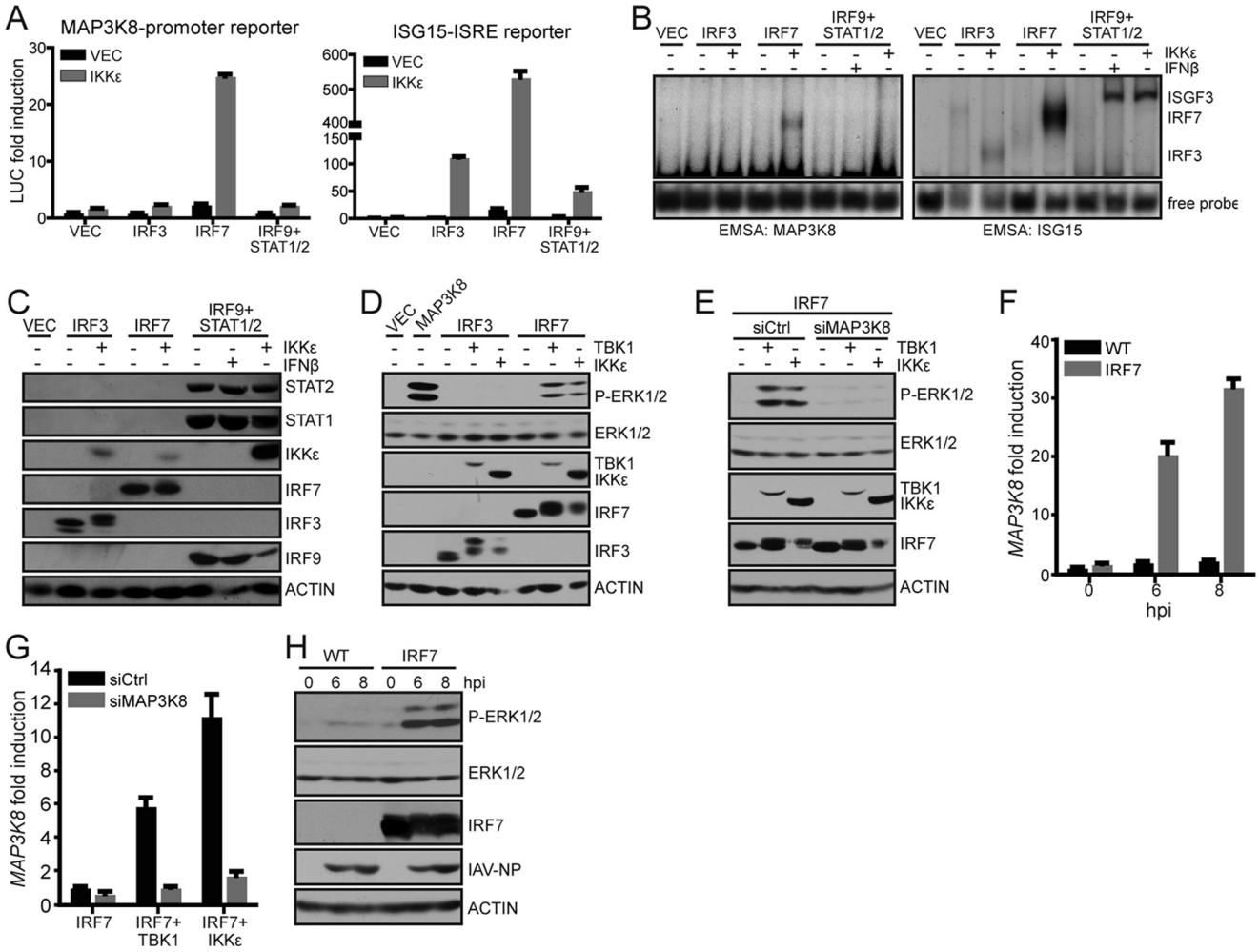

FIGURE 1. **MAP3K8 is induced and activated upon viral infection.** *A*, LUC reporter assay from 293T cells, exogenously expressing IRF3, IRF7, or the components of ISGF3 (STAT1, STAT2, and IRF9) in the presence or absence of IKKε. LUC expression was under the control of the human MAP3K8 promoter (*left panel*) or the ISG15-ISRE (*right panel*). The graphs show average fold induction of LUC over control vector (*VEC*)-treated cells ± S.D. *B*, EMSAs were performed with WCE from 293T cells, exogenously expressing IRF3, IRF7, or the components of ISGF3 in the presence or absence of IKKε. Treatment with IFNβ served to activate ISGF3. Binding of IRF3, IRF7, or ISGF3 to 27-nucleotide-long oligonucleotides comprised either of a sequence from the *MAP3K8* promoter (*left panel*) or of the *ISG15*-ISRE (*right panel*) was analyzed. *C*, WB analysis of WCE as described for *B*. *D*, WB analysis of WCE from 293T cells exogenously expressing IRF3 or IRF7 in the presence or absence of the IRF3/7-activating kinases TBK1 and IKKε. Transfection of MAP3K8 served as positive control. WB shows expression levels of IRF3, IRF7, TBK1, and IKKε as well as total levels of endogenous ERK1/2. Levels of activated ERK1/2 were analyzed with an antibody detecting ERK1/2 phosphorylated at Thr^{202} and Tyr^{204}, or Thr^{185} and Tyr^{187}, respectively (*P-ERK1/2*). *E* and *F*, 293T cells were transfected with expression plasmids for IRF7, TBK1, or IKKε together with a control siRNA (*siCtrl*), or a pool of three siRNAs targeting human *MAP3K8* (*siMAP3K8*). Expression levels of exogenous IRF7, TBK1, and IKKε, as well as endogenous ERK1/2 and P-ERK1/2, were analyzed by WB (*E*), and expression levels of *MAP3K8* transcripts were analyzed by qPCR (*F*). *G* and *H*, WT 293T cells or 293T cells stably expressing IRF7 were infected with an attenuated influenza A virus (*IAV*) harboring two mutations in the double-stranded RNA-binding domain of the nonstructural protein 1 to induce the innate immune response. Total RNA (*G*) and WCE (*H*) were harvested at 0, 6, and 8 hpi and analyzed by qPCR for the induction of *MAP3K8* transcripts (*G*) or by WB for P-ERK-1/2 (*H*). WB was also analyzed for the expression of total ERK1/2, IRF7, and the nucleoprotein (*NP*) of IAV (*H*).

STAT2, and IRF9), induced expression of LUC (Fig. 1*A*, *left panel*). In contrast, LUC under control of the *ISG15*-ISRE was induced by activated IRF3, IRF7, and ISGF3 (Fig. 1*A*, *right panel*). We screened the *MAP3K8* promoter region for putative ISREs or IRF-Es and identified a 27-nucleotide-long sequence that conformed to the known consensus sites for IRF binding (58). Using this sequence, we performed EMSAs with extracts from fibroblasts expressing either IRF3, IRF7, or the components of the ISGF3 complex with or without the IRF3/7 kinase, IKKε (51, 59). Only activated IRF7 bound to the newly identified IRF-E in the human *MAP3K8* promoter, in contrast to a similar enhancer element in *ISG15*, which could be engaged by all three factors (Fig. 1*B*). Expression levels of the transcription factors were determined by WB (Fig. 1*C*).

We next analyzed the activity of IRF7-induced MAP3K8 by examining its known downstream targets. MAP3K8 phosphorylates the MAP2K MEK, which in turn activates the MAPK ERK1/2 (39, 40). To determine ERK1/2 phosphorylation upon induction of MAP3K8, we exogenously expressed either IRF7 or IRF3 together with TBK1 or IKKε. As a positive control, overexpression of MAP3K8 led to high phosphorylation of ERK1/2 (Fig. 1*D*). As expected, only activated IRF7, but not activated IRF3, led to robust activation of ERK1/2 (Fig. 1*D*). To ensure that phosphorylation of ERK1/2 was mediated via MAP3K8, we utilized a pool of three siRNAs targeting *MAP3K8* (siMAP3K8). In response to IRF7 activation, WB analysis showed no phosphorylation of ERK1/2 in the presence of siMAP3K8, despite equal amounts of total ERK1/2 protein (Fig.

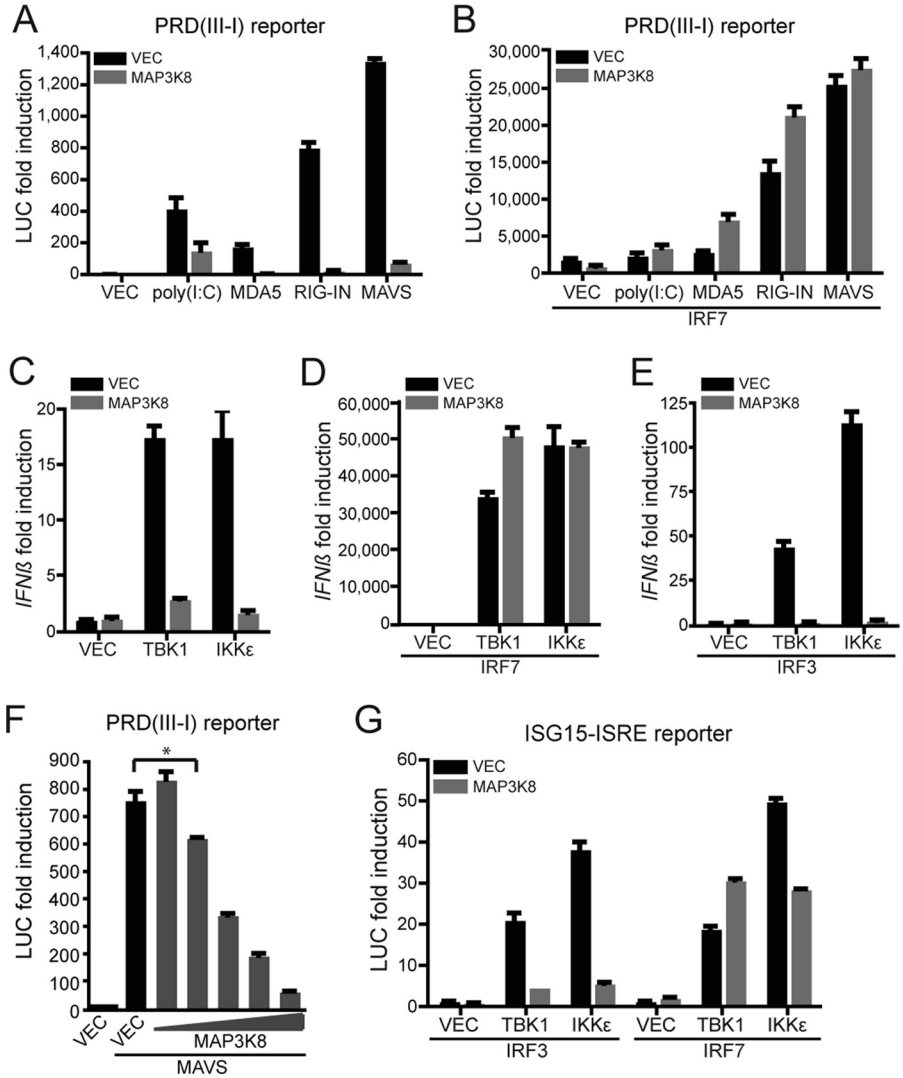

FIGURE 2. **MAP3K8 inhibits IRF3-dependent gene expression.** *A* and *B*, LUC reporter assay from 293T cells transfected with empty vector (*VEC*), poly(I:C), MDA5, constitutively active RIG-I (*RIG-IN*), or MAVS. Additionally, IRF7 was co-transfected in *B*. LUC expression under the control of the PRD(III-I) of the *IFNβ* promoter was analyzed in the presence and absence of exogenous MAP3K8. The graphs show average fold induction of LUC over vector-treated cells ± S.D. *C–E*, expression of *IFNβ* transcripts in the presence and absence of exogenous MAP3K8 was analyzed by qPCR in 293T cells exogenously expressing TBK1 or IKKε (*C*), TBK1 or IKKε together with IRF7 (*D*), or TBK1 or IKKε together with IRF3 (*E*). The graphs show fold induction over vector-treated cells ± S.D. *F*, LUC reporter assay from 293T cells exogenously expressing MAVS together with increasing amounts of MAP3K8. LUC expression was under the control of the PRD(III-I) of the *IFNβ* promoter. The graphs show average fold induction of LUC over VEC-treated cells ± S.D. *, $p < 0.02$, as determined using a two-tailed, unpaired Student's *t* test. *G*, LUC reporter assay from 293T cells, exogenously expressing TBK1 or IKKε together with IRF3 or IRF7 in the presence or absence of MAP3K8. LUC expression was under the control of the *ISG15*-ISRE. The graph shows average fold induction of LUC over VEC-treated cells ± S.D.

1*E*). Complete silencing of MAP3K8 by siMAP3K8 was confirmed by qPCR (Fig. 1*F*). Furthermore, fibroblasts stably expressing IRF7 induced high amounts of *MAP3K8* transcripts and phosphorylated ERK1/2 at 6 and 8 hpi with a mutated influenza A virus lacking a functional antiviral antagonist (Fig. 1, *G* and *H*). These exciting results suggest that IRF7-induced MAP3K8 is required for the downstream activation of ERK1/2 in response to virus infection.

MAP3K8 Inhibits IRF3-dependent Gene Expression—In addition to the downstream activation of ERK1/2, MAP3K8 was previously implicated in the regulation of IFNβ production in macrophages and dendritic cells stimulated with a bacterial PAMP (44, 46, 47). However, it remained unclear how this regulation was achieved or whether MAP3K8 also regulates IFNβ expression in response to diverse pattern recognition receptor activation. We therefore analyzed whether MAP3K8 influenced IFNβ expression in fibroblasts upon viral infection. We utilized a LUC reporter construct, with LUC under control of the positive regulatory domains III and I (PRD(III-I)) of the IFNβ promoter, which are the binding sites for IRF3 and IRF7 (5). Not surprisingly, exogenous expression of the pattern recognition receptor MDA5, constitutively active RIG-I (RIG-IN), or MAVS, as well as transfection with poly(I:C), a mimic of viral PAMPs, led to robust expression of LUC (Fig. 2*A*). However, simultaneous expression of MAP3K8 significantly inhibited LUC expression (Fig. 2*A*). Interestingly, the negative impact of MAP3K8 on PRD(III-I) could be counteracted by the additional expression of IRF7 (Fig. 2*B*). In agreement with the LUC data, expression of MAP3K8 could also inhibit induction of endogenous IFNβ (Fig. 2*C*). Furthermore, enhanceosome activity

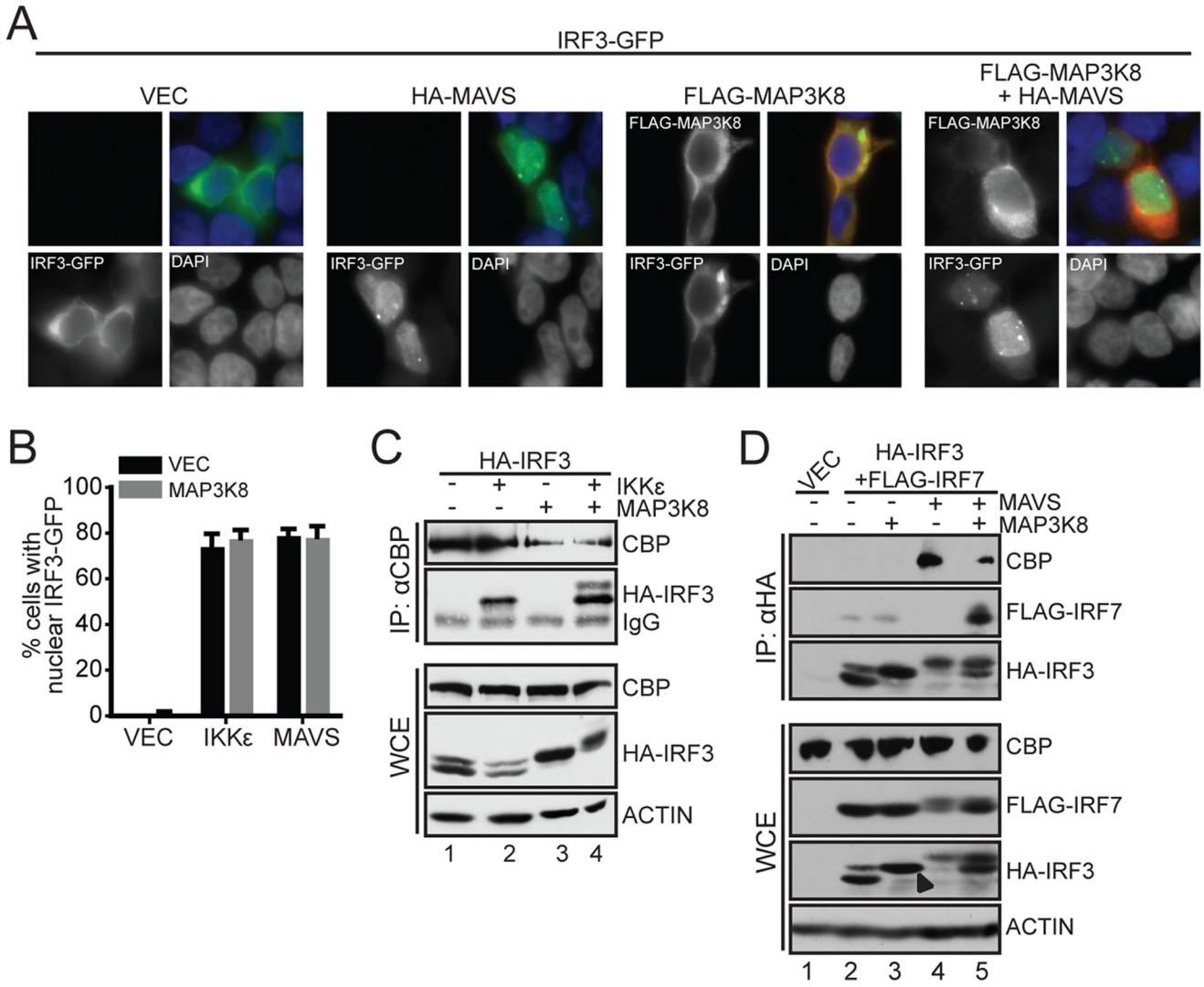

FIGURE 3. **MAP3K8 promotes formation of IRF3:IRF7 dimers.** *A*, immunofluorescence analysis of 293T cells exogenously expressing an IRF3-GFP fusion construct, together with HA-MAVS and FLAG-MAP3K8 in the indicated combinations. In the overlay, IRF3-GFP is shown in *green*, FLAG-MAP3K8 is in *red*, and DAPI is in *blue*. *B*, the graph shows the percentage of cells with nuclear IRF3-GFP in the presence and absence of exogenous MAP3K8. Nuclear IRF3-GFP was analyzed by immunofluorescence analysis as shown in *A*. Nuclear translocation of IRF3-GFP was induced by expression of either IKKε or MAVS. Shown is the average ± S.D. of three independent fields. *C*, coIP of CBP from WCE derived from 293T cells exogenously expressing HA-IRF3, IKKε, and MAP3K8 in the indicated combinations. WB was analyzed for HA-IRF3 as well as endogenous CBP and ACTIN. *D*, coIP of HA-IRF3 from WCE derived from 293T cells exogenously expressing HA-IRF3, FLAG-IRF7, MAVS, and MAP3K8 in the indicated combinations. WB was analyzed for HA-IRF3 and FLAG-IRF7 as well as endogenous CBP and ACTIN.

could be restored in the presence of MAP3K8 by exogenous expression of IRF7 (Fig. 2*D*), but not IRF3 (Fig. 2*E*). The negative effect of MAP3K8 on IRF3-regulated gene expression was dose-dependent and evident at physiological levels of MAP3K8 (Fig. 2*F*). We further analyzed whether MAP3K8 exhibited the same effect on other IRF3-regulated genes, such as ISG15. Indeed, MAP3K8 inhibited the expression of LUC under control of the IRF-E of *ISG15* only in the presence of IRF3, whereas exogenous expression of IRF7 again rescued the phenotype (Fig. 2*G*). These data suggest that MAP3K8 may be restricting the use of IRF3 to utilize the greater transcriptional potential of IRF7 in the context of virus infection.

MAP3K8 Promotes Formation of IRF3:IRF7 Dimers—Upon detection of viral PAMPs, the C-terminal regulatory domain of IRF3 is phosphorylated causing a change in conformation that promotes homodimer formation, nuclear retention, DNA binding, and recruitment of histone acetyl transferases (60, 61). We first examined whether MAP3K8 impacted the nuclear import of IRF3 by exogenously expressing an IRF3-GFP fusion construct together with MAP3K8 in the context of an active antiviral response. Immunofluorescence analysis of unstimulated cells showed cytoplasmic IRF3-GFP, whereas exogenous expression of MAVS led to nuclear relocalization (Fig. 3*A*). Interestingly, simultaneous expression of MAP3K8 did not inhibit the nuclear accumulation of IRF3-GFP upon its activation (Fig. 3*A*). Quantification of IRF3-GFP confirmed that upon expression of either IKKε or MAVS roughly 80% of the IRF3-GFP positive cells showed nuclear accumulation regardless of MAP3K8 expression (Fig. 3*B*). These data suggest that MAP3K8 does not impact IKK-related activation and subsequent nuclear translocation of IRF3.

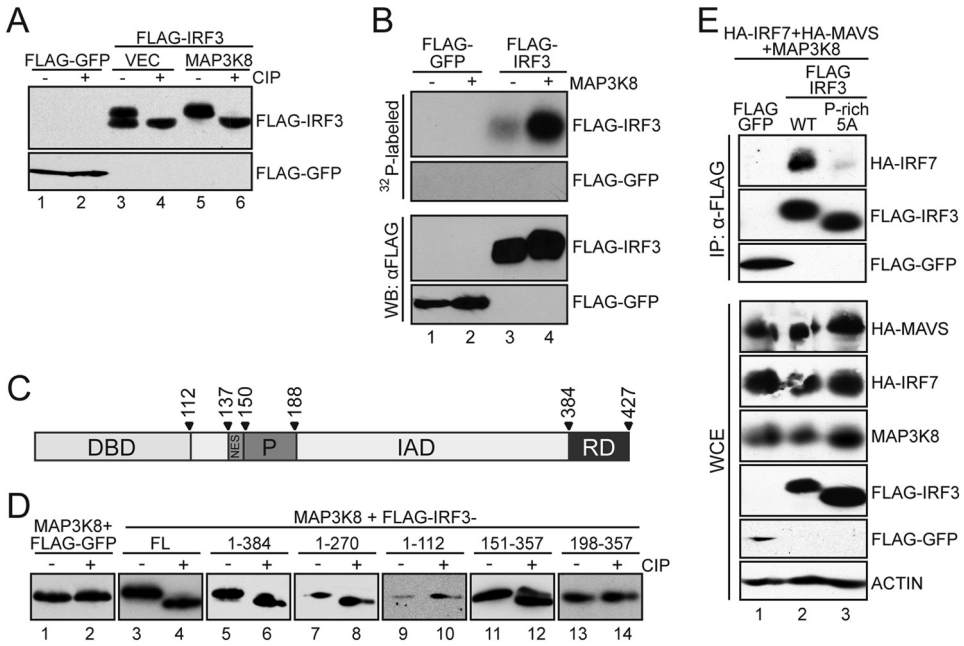

FIGURE 4. **MAP3K8 phosphorylates IRF3 to promote association with IRF7.** *A*, 293T cells were transfected with FLAG-GFP or FLAG-IRF3 with or without MAP3K8. FLAG-tagged proteins were immunoprecipitated using a FLAG-specific antibody and eluted from the beads with FLAG peptide. Half of the eluate was subsequently treated with CIP to remove phosphorylation of proteins. WB was analyzed for FLAG-tagged proteins with or without CIP treatment. *B*, 293T cells were transfected with FLAG-GFP or FLAG-IRF3 with or without MAP3K8. One set of transfected cells was incubated with [^{32}P]ATP for 4 h before harvesting WCE to radiolabel phosphorylated residues. FLAG-tagged proteins were immunoprecipitated using a FLAG-specific antibody and eluted from the beads with FLAG peptide. Eluates were analyzed by SDS-PAGE and either directly exposed to a film (^{32}P-labeled) or detected with a FLAG-specific antibody (*WB: αFLAG*). *C*, the schematic depicts the domain organization of IRF3. *Numbers* give the end and start of each domain. *D*, full-length (*FL*) FLAG-IRF3 or FLAG-tagged truncation mutants of IRF3 were transfected with MAP3K8 into 293T cells. After IP with a FLAG-specific antibody, eluate was divided and either left untreated or incubated with CIP. To reach optimal resolution for each of the truncation mutants, they were analyzed by SDS-PAGE using gels with varying polyacrylamide concentrations. $IRF3_{wt}$ (47 kDa) and $IRF3_{1-384}$ (43 kDa) were run on an 8% gel, $IRF3_{151-357}$ (23 kDa) was run on a 10% gel, and $IRF3_{1-270}$ (30 kDa), $IRF3_{1-112}$ (13 kDa), and $IRF3_{198-357}$ (18 kDa) were run on a 15% gel. *E*, coIP of FLAG-$IRF3_{wt}$ or FLAG-$IRF3_{P\text{-}rich\text{-}5A}$ from WCE derived from 293T cells exogenously expressing HA-IRF7, HA-MAVS, and MAP3K8. WB was analyzed for the levels of proteins in the IP fraction and WCE.

In contrast to IRF3, IRF7 exhibits intrinsic transcriptional activity that does not depend on the co-activators p300 or CBP to induce gene expression (31, 62). We therefore next analyzed whether the IRF3/histone acetyl transferase association was impacted in the presence of MAP3K8. To this end, we performed co-immunoprecipitation (coIP) experiments with WCE from fibroblasts expressing epitope-tagged IRF3 and MAP3K8 in the presence and absence of an active antiviral response (Fig. 3*C*). As expected, we observed association between active IRF3 and CBP (Fig. 3*C*). Furthermore, histone acetyl transferase association was not impacted by the additional expression of MAP3K8, suggesting that loss of IRF3 transcriptional activity must occur at the level of enhancer engagement.

It is well established that IRF3 and IRF7 can form homo- as well as heterodimers (63, 64), the latter being essential for robust induction of IFNβ (21, 65). However, the mechanism by which formation of the different dimers is regulated remains unknown. We wondered whether MAP3K8 would influence the ability of IRF3 to form homo- or heterodimers, which would then impact the expression of IRF3:IRF3- or IRF3:IRF7-driven genes, such as IFNβ. To test this hypothesis, we performed coIP analysis of WCE from fibroblasts exogenously expressing the indicated genes. As previously described (63), low levels of heterodimer formation were detectable in the absence of stimulus but were eliminated upon IRF3 activation, presumably because of dominant production of IRF3:IRF3 (Fig. 3*D*). Expression of MAP3K8 did not significantly change formation of basal heterodimer binding; however, MAP3K8 strongly promoted formation of IRF3:IRF7 upon their activation (Fig. 3*D*). In agreement with increased formation of IRF3:IRF7, coIP of CBP was reduced in the presence of MAP3K8 (Fig. 3*D*) because this histone acetyl transferase would now only associate with a single Ser^{396} phosphorylation event (66). Taken together, these results suggest that MAP3K8 does not block the canonical C-terminal phosphorylation of IRF3 nor impact nuclear translocation, but instead promotes IRF3:IRF7 formation, thereby increasing the binding capacity of this virus response complex.

MAP3K8 Mediates Phosphorylation of IRF3 to Promote Association with IRF7—In our efforts to ascertain how MAP3K8 was inhibiting IRF3 transcriptional potential, evidence for additional post-translational modifications became apparent as IRF3, but not IRF7, migrated slower by gel electrophoresis in the presence of the kinase (Fig. 3*D*, *arrowhead*). To determine whether the change in mobility was the result of phosphorylation, we used two different methods. First, we treated epitope-tagged IRF3 with CIP. Under resting conditions, IRF3 is a doublet as a result of N-terminal phospho-residues of unknown function (66). In the presence of MAP3K8, IRF3 exists only as a higher migrating form (Fig. 4*A*). In contrast, CIP treatment of IRF3 shifts the protein population to only the lower form, suggesting that MAP3K8 influences the phosphorylation status of this transcription factor (Fig. 4*A*). Furthermore, *in vivo* labeling

using [^{32}P]ATP confirmed that expression of MAP3K8 leads to robust phosphorylation of IRF3 (Fig. 4*B*).

To refine the MAP3K8-induced modification of IRF3, we generated several deletion mutants to narrow down where phosphorylation was occurring based on the known structural elements of this transcription factor (Fig. 4*C*). C-terminal deletion of the regulatory domain ($IRF3_{1-384}$) or disruption of the IRF-association domain (IAD, $IRF3_{1-270}$) did not impact MAP3K8-mediated IRF3 phosphorylation, suggesting that the target site(s) were in the first 270 residues (Fig. 4*D*). However, the DNA-binding domain of IRF3 ($IRF3_{1-112}$), which also demonstrated poor stability, was no longer phosphorylated in response to MAP3K8, suggesting that the target region is contained between residues 112 and 270, encompassing the proline-rich region (Fig. 4, *C* and *D*). To further define the MAP3K8 impacted area, we generated two additional constructs that either contained or eliminated this characterized "hinge" region. $IRF3_{151-357}$ showed evidence for MAP3K8-induced phosphorylation, whereas $IRF3_{198-357}$ did not (Fig. 4*D*), implicating that the observed changes in mobility were the result of phosphorylation in the P-rich hinge region.

In addition to proline, the hinge region also contains a cluster of serines and threonines including Ser^{173}, Ser^{175}, Thr^{180}, and Ser^{188}. Interestingly, Ser^{175} and Thr^{180} together with Ser^{123} were previously described to be phosphorylated by the Epstein-Barr virus kinase BGLF4 (67), which led to inhibition of transcriptional activity of IRF3. As such, we substituted these amino acids as well as Ser^{173} and Ser^{188} to alanines ($IRF3_{P\text{-}rich\text{-}5A}$) and analyzed the interaction of $IRF3_{P\text{-}rich\text{-}5A}$ with IRF7 by coIP. Excitingly, we observed robust formation of $IRF3_{wt}$:IRF7 dimers in the presence of MAP3K8, but the interaction between IRF7 and $IRF3_{P\text{-}rich\text{-}5A}$ was markedly reduced (Fig. 4*E*). It is noteworthy that this P-rich region is distinct from the essential residues implicated in binding IRF7 (aa306–357) (63, 68). However, the crystal structure of IRF dimers suggests that the P-rich region is in close proximity with the dimer interface (69), making intermolecular interactions possible. Taken together, these data show that MAP3K8 either directly or indirectly leads to phosphorylation of IRF3 in the P-rich hinge region, which increases the formation of IRF3:IRF7 and affects downstream gene induction.

MAP3K8 Is Required to Limit Virus Replication—IRF3 and IRF7 are essential transcription factors in the immediate antiviral response, not only for the induction of IFN-I, but also for establishment of the antiviral state (20, 32, 65). We therefore speculated that assembling IRF3 into different complexes (*i.e.*, IRF3:IRF3 or IRF3:IRF7) should alter the virus-induced transcriptome, rendering cells more permissive to infection should the MAP3K8/IRF7 axis be disrupted. To test this hypothesis, we infected $Map3k8^{+/+}$ or $Map3k8^{-/-}$ fibroblasts at an MOI of 0.01 with a vesicular stomatitis virus unable to shut down nuclear export of host transcripts (VSV-M51R) (49). Growth analysis over 48 hpi showed a significant increase of viral titers in $Map3k8^{-/-}$ fibroblasts (Fig. 5*A*). In agreement with these data, levels of VSV glycoprotein in $Map3k8^{-/-}$ fibroblasts were significantly enhanced at 12 hpi (Fig. 5*B*). These data are consistent with the hypothesis that MAP3K8 plays an important role in the antiviral defense.

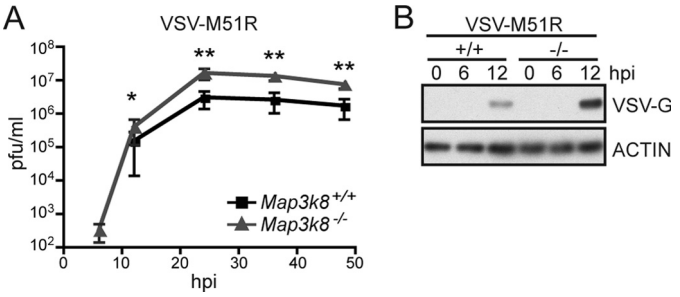

FIGURE 5. **MAP3K8 is required to limit virus replication.** *A*, $Map3k8^{+/+}$ and $Map3k8^{-/-}$ fibroblasts were infected at an MOI of 0.01 with an attenuated vesicular stomatitis virus (VSV-M51R) that is unable to shutdown nuclear export of host transcripts because of an amino acid substitution in the matrix protein. The graph shows viral titers over the course of 48 hpi. Shown are average plaque forming units (*pfu*)/ml ± S.D. *, $p < 0.003$; **, $p < 0.0002$ as determined using a two tailed, unpaired Student's *t* test. *B*, WB analysis of fibroblasts infected as described for *A*. Shown are expression levels of the VSV glycoprotein (*VSV-G*) and ACTIN.

MAP3K8 Reinforces the Antiviral Transcriptome—Next, to delineate the role of MAP3K8 in response to virus infection, we performed mRNA-seq analysis of VSV-M51R infected $Map3k8^{+/+}$ and $Map3k8^{-/-}$ fibroblasts. This analysis demonstrated that the virus infection induced ~70 genes to a higher level in $Map3k8^{+/+}$ compared with $Map3k8^{-/-}$ fibroblasts (Fig. 6*A*). Included in this transcriptional profile were virus-induced genes, as well as transcripts previously described to be regulated by IRF7, such as *Ifnα* subtypes and ISGs such as *Oas2/3*, *Herc6*, and *Gbp6*. Notably, among the genes demonstrating significant disparities between genotypes, three members of the SP100 nuclear antigen family, *Sp100*, *Sp110*, and *Sp140*, were expressed ~5 times higher in $Map3k8^{+/+}$ fibroblasts. These data were corroborated by qPCR (Fig. 6*B*).

SP100 family members are components of promyelocytic leukemia nuclear bodies (PML-NBs), which are subnuclear structures that have been implicated in a range of cellular processes including: innate immunity, apoptosis, antiviral responses, and oncogenesis (70–72). To analyze whether IRF7 induces expression of this gene family, we first performed EMSA analysis, using previously identified IRF-Es of the promoters of *SP100* and *SP110* (73, 74). Only activated IRF7 was capable of engaging these elements (Fig. 6*C*). In agreement with these data, qPCR analysis of human fibroblasts exogenously expressing activated IRF7 showed an ~40-fold induction of two splice variants of *SP100* as well as of *SP110* (Fig. 6*D*).

The Antiviral Activity of the IRF7/MAP3K8 Axis Is Aided by SP100B/C—PML-NBs are known to associate with transcriptionally active genomic regions; however, their exact molecular function during transcription is largely unknown (75). We hypothesized that SP100C and SP100B might influence the transcriptional level of *IFNβ* during viral infection, given how the loss of MAP3K8 resulted in a dramatic reduction of interferon response genes (Fig. 6*A*). To test our hypothesis, we exogenously expressed MAVS to induce *IFNβ* transcription (76) in the presence or absence of SP100C or SP100B. As expected, expression of SP100C or SP100B independently did not induce *IFNβ* (Fig. 7*A*). However, co-expression of MAVS with SP100C or SP100B led to a ~5-fold increase of *IFNβ* transcripts compared with MAVS only (Fig. 7*A*). We next ascertained whether this transcriptional dichotomy was a component of the under-

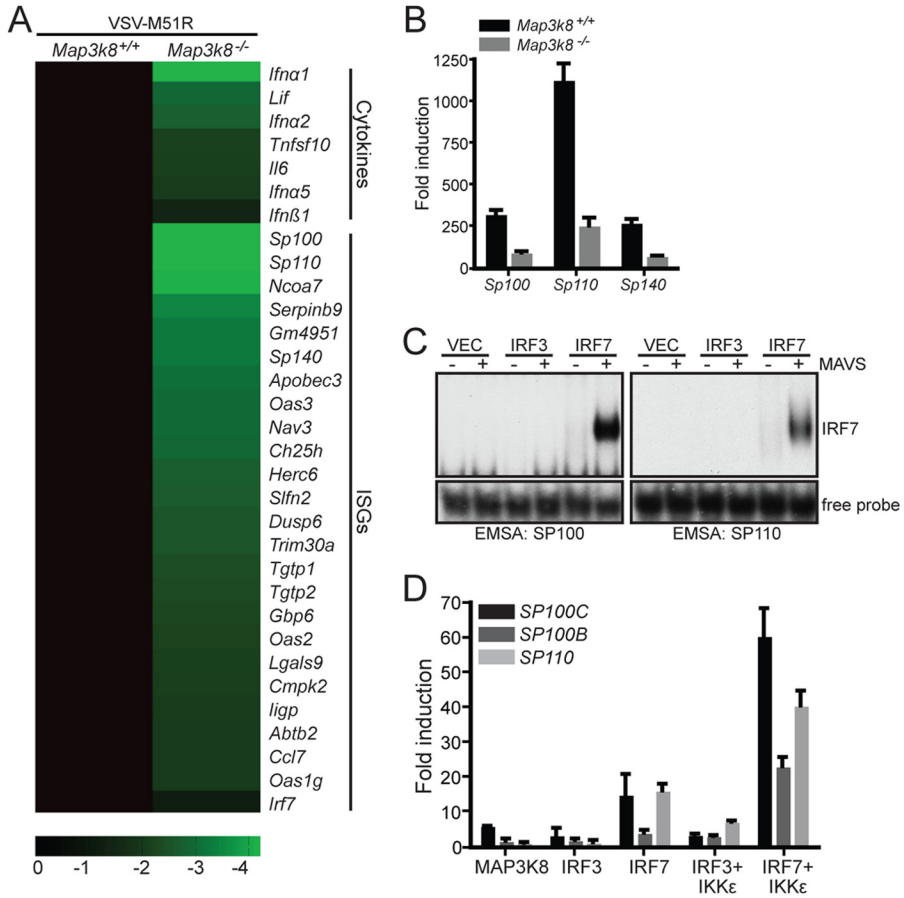

FIGURE 6. **MAP3K8 reinforces the antiviral transcriptome.** *A*, *Map3k8*$^{+/+}$ and *Map3k8*$^{-/-}$ fibroblasts were infected at an MOI of 1 with VSV-M51R, and their mRNA expression profile was analyzed by mRNA-seq at 10 hpi. The heat map shows cytokines and ISGs that were at least 4-fold induced in VSV-infected over mock infected fibroblasts. *B*, qPCR analysis of *Sp100*, *Sp110*, and *Sp140* transcripts in *Map3k8*$^{+/+}$ and *Map3k8*$^{-/-}$ fibroblasts, 10 hpi (MOI 1) with VSV-M51R. *C*, WCE from 293T cells exogenously expressing IRF3, IRF7, and MAVS in the indicated combinations was analyzed for DNA binding by EMSA. The used probes contained the IRF-Es from the promoters of human *SP100* and *SP110*. *D*, qPCR analysis of *SP100C*, *SP100B*, and *SP110* transcripts in 293T cells exogenously expressing MAP3K8, IRF3, IRF7, and IKKε in the indicated combinations. The graph shows average fold induction over control vector (*VEC*)-treated cells ± S.D.

lying molecular mechanism that increased virus replication levels in *Map3k8*$^{-/-}$ fibroblasts. To this end, we expressed SP100C and SP100B and subsequently infected these cells with VSV at an MOI of 0.1. As a positive control, we expressed MAVS. Excitingly, expression of SP100C or SP100B significantly reduced VSV titers by almost a full log, mirroring the inverse correlation to that observed in *Map3k8*$^{-/-}$ fibroblasts (Fig. 7*B*). These titer data could further be corroborated at a protein level (Fig. 7*C*). Consistent with increased *IFNβ* transcription, expression of STAT1, a critical ISG, was increased in cells expressing SP100C or B, as compared with vector-treated cells (Fig. 7*C*). Taken together, these data illustrate that the MAP3K8/IRF7 axis is an essential amplification component of the antiviral response needed to successfully suppress unabated virus replication.

DISCUSSION

Chordates are continuously infected by viruses with a wide spectrum of outcomes, ranging from immediate clearance to severe disease. To ensure the appropriate strength of the response, a complex network with positive and negative feedback loops has evolved (11, 77, 78). This network structure guarantees robust activation of the antiviral response only in the case of viral replication (79–82). We have identified such a positive feedback loop that ensures a superior transcriptional response in the case of sustained viral replication. IRF3 is among the first transcription factors activated by PAMP recognition and induces low amounts of IFNβ through a stochastic process, because the enhanceosome is not optimized for IRF3 dimers (21, 65). However, small amounts of IFNβ result in the up-regulation of IRF7, which in turn allows for amplification of IFN-I, so long as PAMP is still present to mediate upstream kinase activation. In addition to amplifying IFN-I, IRF7 activation also results in the up-regulation of a small subset of specific target genes including MAP3K8. Here we show that MAP3K8 licenses IRF7 function by providing this transcription factor with IRF3 as a binding partner. This biological activity then generates an IRF complex capable of impacting a much greater transcriptional response on IRF-Es than the more stringent binding of IRF3 dimers could ever perform. This change in transcription factor utility essentially ensures that the response to virus correlates to the pathogenic threat by increasing transcriptional targets proportionally with the sustained time of PAMP production. It is also important to consider that this phenomenon is not limited to IRF7 and may include other IRFs such as IRF1. In this regard, it is interesting to note that IRF1 was recently found to be one of the more essential IRFs in con-

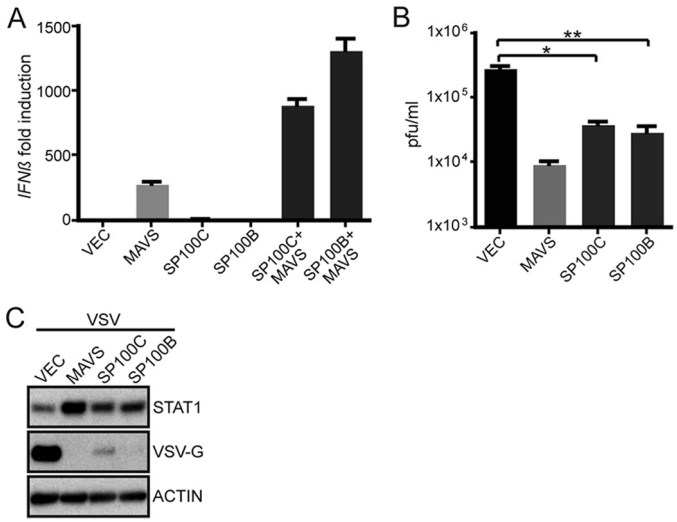

FIGURE 7. **The antiviral activity of the IRF7/MAP3K8 axis is aided by SP100B/C.** *A*, qPCR analysis of *IFNβ* transcripts in 293T cells exogenously expressing MAVS, SP100C, and SP100B in the indicated combinations. The graph shows average fold induction over vector-treated cells ± S.D. *B*, 2FTGH cells were transfected with either empty vector (*VEC*), MAVS, SP100C, or SP100B. 30 hpt, cells were infected with wild-type VSV at an MOI of 0.1. Titers in the supernatant were determined at 16 hpi. *, $p < 0.02$; **, $p < 0.007$, as determined using a two-tailed, unpaired Student's *t* test. *C*, WB analysis of cells treated as in *B* at 16 hpi. Shown are expression levels of STAT1, VSV-G, and ACTIN.

trolling virus infection and was implicated in the induction of SP100 genes (8). Future work will be needed to address this directly.

Here we show that SP100, SP110, and SP140, which are key components of PML-NBs, are effectively induced by the IRF7/MAP3K8 axis in response to sustained infection environments. Furthermore, we show that overexpression of SP100C or SP100B inhibits VSV replication. We investigated the antiviral mechanism of SP100C and SP100B. We show here for the first time that SP100C and SP100B increase IFNβ expression during the antiviral response. This finding is consistent with the known association of PML-NBs with transcriptionally active genomic regions (75). For example, with regards to the MHC locus, PML-NBs are essential for IFNγ induced expression of MHC genes (83, 84). The regulation is achieved through formation of dynamic chromatin loops and the stabilization of transactivators. We show here that IFNβ is another genomic locus that is positively regulated by PML-NBs through SP100C or SP100B. Interestingly, both loci, MHC and IFNβ, need to be tightly regulated in healthy conditions but highly induced during an antiviral response. Taken together, the regulation of PML-NBs by the IRF7/MAP3K8 axis may ensure optimal gene induction in the case of extended viral replication to ultimately clear the virus.

Interestingly, ERK, a downstream target of MAP3K8, was also implicated in the assembly of PML-NBs (85). Given that we demonstrated that MAP3K8 was essential for ERK activation in response to virus, these results suggest that the cellular environment during this antiviral program is significantly interconnected. Sustained IRF7 activation results in MAP3K8 up-regulation and activation. Subsequently, MAP3K8 further promotes IRF7-mediated induction of SP100 family members whose assembly into PML-NBs is coordinated by the activation of ERK, which is also mediated by MAP3K8. The integrated nature of this pathway suggests that it may play a critical role in the cellular response to infection. In support of this concept, $Pml^{-/-}$ mice are more susceptible to infection with VSV and lymphocytic choriomeningitis virus (86), and overexpression of PML inhibits replication of VSV, rabies virus, and influenza A virus (87–89). Further indirect evidence for an antiviral role of PML-NBs comes from the observation that several RNA and DNA viruses disrupt PML-NBs (90). In this regard, it is interesting that *Drosophila* also utilizes an ERK-based pathway to control virus infection (91) and encodes an SP100 homolog, suggesting that this pathway may represent a conserved and critical means to reinforce the cellular response reserved for imminent threats to the host.

Acknowledgments—The following reagents were obtained through BEI Resources, NIAID, National Institutes of Health: human interferon β (HuIFN-β), NR-3080, and monoclonal anti-influenza A virus NP, clone IC5–1B7 (produced in vitro), NR-4544. Map3k8$^{+/+}$ and Map3k8$^{-/-}$ fibroblasts were a kind gift from Dr. Philip N. Tsichlis (Thomas Jefferson University, Philadelphia, PA). Plasmids encoding for EYFP fused human SP100B and SP100C were a kind gift from Dr. Susan M. Janicki (Wistar Institute, Philadelphia, PA). Plasmids encoding for IRF3$_{151-357}$ and IRF3$_{198-357}$ were a kind gift of Dr. Rongtuan Lin (McGill University, Montreal, Canada). We thank the Genomics Core Facility at Icahn Institute for Genomics and Multiscale Biology at Mount Sinai for next generation sequencing.

REFERENCES

1. Akira, S., Uematsu, S., and Takeuchi, O. (2006) Pathogen recognition and innate immunity. *Cell* **124,** 783–801
2. Alexopoulou, L., Holt, A. C., Medzhitov, R., and Flavell, R. A. (2001) Recognition of double-stranded RNA and activation of NF-κB by Toll-like receptor 3. *Nature* **413,** 732–738
3. Meylan, E., Tschopp, J., and Karin, M. (2006) Intracellular pattern recognition receptors in the host response. *Nature* **442,** 39–44
4. Levy, D. E., Marié, I. J., and Durbin, J. E. (2011) Induction and function of type I and III interferon in response to viral infection. *Curr. Opin. Virol.* **1,** 476–486
5. Maniatis, T., Falvo, J. V., Kim, T. H., Kim, T. K., Lin, C. H., Parekh, B. S., and Wathelet, M. G. (1998) Structure and function of the interferon-β enhanceosome. *Cold Spring Harb. Symp. Quant. Biol.* **63,** 609–620
6. Darnell, J. E., Jr., Kerr, I. M., and Stark, G. R. (1994) Jak-STAT pathways and transcriptional activation in response to IFNs and other extracellular signaling proteins. *Science* **264,** 1415–1421
7. Li, J., Ding, S. C., Cho, H., Chung, B. C., Gale, M., Jr., Chanda, S. K., and Diamond, M. S. (2013) A short hairpin RNA screen of interferon-stimulated genes identifies a novel negative regulator of the cellular antiviral response. *MBio* **4,** e00385–e00313
8. Schoggins, J. W., Wilson, S. J., Panis, M., Murphy, M. Y., Jones, C. T., Bieniasz, P., and Rice, C. M. (2011) A diverse range of gene products are effectors of the type I interferon antiviral response. *Nature* **472,** 481–485
9. Sadler, A. J., and Williams, B. R. (2008) Interferon-inducible antiviral effectors. *Nat. Rev. Immunol.* **8,** 559–568
10. Ireton, R. C., and Gale, M., Jr. (2011) RIG-I like receptors in antiviral immunity and therapeutic applications. *Viruses* **3,** 906–919
11. Yoshimura, A., Naka, T., and Kubo, M. (2007) SOCS proteins, cytokine signalling and immune regulation. *Nat. Rev. Immunol.* **7,** 454–465
12. Mamane, Y., Heylbroeck, C., Génin, P., Algarté, M., Servant, M. J., LePage, C., DeLuca, C., Kwon, H., Lin, R., and Hiscott, J. (1999) Interferon regulatory factors. The next generation. *Gene* **237,** 1–14
13. Harada, H., Takahashi, E., Itoh, S., Harada, K., Hori, T. A., and Taniguchi, T. (1994) Structure and regulation of the human interferon regulatory

factor 1 (IRF-1) and IRF-2 genes. Implications for a gene network in the interferon system. *Mol. Cell Biol.* **14,** 1500–1509
14. Feng, D., Sangster-Guity, N., Stone, R., Korczeniewska, J., Mancl, M. E., Fitzgerald-Bocarsly, P., and Barnes, B. J. (2010) Differential requirement of histone acetylase and deacetylase activities for IRF5-mediated proinflammatory cytokine expression. *J. Immunol.* **185,** 6003–6012
15. Lazear, H. M., Lancaster, A., Wilkins, C., Suthar, M. S., Huang, A., Vick, S. C., Clepper, L., Thackray, L., Brassil, M. M., Virgin, H. W., Nikolich-Zugich, J., Moses, A. V., Gale, M., Jr., Früh, K., and Diamond, M. S. (2013) IRF-3, IRF-5, and IRF-7 coordinately regulate the type I IFN response in myeloid dendritic cells downstream of MAVS signaling. *PLoS Pathog.* **9,** e1003118
16. Veals, S. A., Schindler, C., Leonard, D., Fu, X. Y., Aebersold, R., Darnell, J. E., Jr., and Levy, D. E. (1992) Subunit of an α-interferon-responsive transcription factor is related to interferon regulatory factor and Myb families of DNA-binding proteins. *Mol. Cell Biol.* **12,** 3315–3324
17. Génin, P., Lin, R., Hiscott, J., and Civas, A. (2009) Differential regulation of human interferon A gene expression by interferon regulatory factors 3 and 7. *Mol. Cell Biol.* **29,** 3435–3450
18. Barnes, B. J., Richards, J., Mancl, M., Hanash, S., Beretta, L., and Pitha, P. M. (2004) Global and distinct targets of IRF-5 and IRF-7 during innate response to viral infection. *J. Biol. Chem.* **279,** 45194–45207
19. Chattopadhyay, S., Fensterl, V., Zhang, Y., Veleeparambil, M., Yamashita, M., and Sen, G. C. (2013) Role of interferon regulatory factor 3-mediated apoptosis in the establishment and maintenance of persistent infection by Sendai virus. *J. Virol.* **87,** 16–24
20. Schmid, S., Mordstein, M., Kochs, G., García-Sastre, A., and Tenoever, B. R. (2010) Transcription factor redundancy ensures induction of the antiviral state. *J. Biol. Chem.* **285,** 42013–42022
21. Panne, D., Maniatis, T., and Harrison, S. C. (2007) An atomic model of the interferon-β enhanceosome. *Cell* **129,** 1111–1123
22. Escalante, C. R., Nistal-Villán, E., Shen, L., García-Sastre, A., and Aggarwal, A. K. (2007) Structure of IRF-3 bound to the PRDIII-I regulatory element of the human interferon-β enhancer. *Mol. Cell* **26,** 703–716
23. Grandvaux, N., Servant, M. J., tenOever, B., Sen, G. C., Balachandran, S., Barber, G. N., Lin, R., and Hiscott, J. (2002) Transcriptional profiling of interferon regulatory factor 3 target genes. Direct involvement in the regulation of interferon-stimulated genes. *J. Virol.* **76,** 5532–5539
24. Tanaka, N., Kawakami, T., and Taniguchi, T. (1993) Recognition DNA sequences of interferon regulatory factor 1 (IRF-1) and IRF-2, regulators of cell growth and the interferon system. *Mol. Cell Biol.* **13,** 4531–4538
25. Fujii, Y., Shimizu, T., Kusumoto, M., Kyogoku, Y., Taniguchi, T., and Hakoshima, T. (1999) Crystal structure of an IRF-DNA complex reveals novel DNA recognition and cooperative binding to a tandem repeat of core sequences. *EMBO J.* **18,** 5028–5041
26. Veals, S. A., Santa Maria, T., and Levy, D. E. (1993) Two domains of ISGF3γ that mediate protein-DNA and protein-protein interactions during transcription factor assembly contribute to DNA-binding specificity. *Mol. Cell Biol.* **13,** 196–206
27. Sato, M., Suemori, H., Hata, N., Asagiri, M., Ogasawara, K., Nakao, K., Nakaya, T., Katsuki, M., Noguchi, S., Tanaka, N., and Taniguchi, T. (2000) Distinct and essential roles of transcription factors IRF-3 and IRF-7 in response to viruses for IFN-α/β gene induction. *Immunity* **13,** 539–548
28. Marié, I., Durbin, J. E., and Levy, D. E. (1998) Differential viral induction of distinct interferon-α genes by positive feedback through interferon regulatory factor-7. *EMBO J.* **17,** 6660–6669
29. Taniguchi, T., Ogasawara, K., Takaoka, A., and Tanaka, N. (2001) IRF family of transcription factors as regulators of host defense. *Annu. Rev. Immunol.* **19,** 623–655
30. Morin, P., Bragança, J., Bandu, M. T., Lin, R., Hiscott, J., Doly, J., and Civas, A. (2002) Preferential binding sites for interferon regulatory factors 3 and 7 involved in interferon-A gene transcription. *J. Mol. Biol.* **316,** 1009–1022
31. Lin, R., Génin, P., Mamane, Y., and Hiscott, J. (2000) Selective DNA binding and association with the CREB binding protein coactivator contribute to differential activation of α/β interferon genes by interferon regulatory factors 3 and 7. *Mol. Cell Biol.* **20,** 6342–6353
32. Honda, K., Yanai, H., Negishi, H., Asagiri, M., Sato, M., Mizutani, T., Shimada, N., Ohba, Y., Takaoka, A., Yoshida, N., and Taniguchi, T. (2005) IRF-7 is the master regulator of type-I interferon-dependent immune responses. *Nature* **434,** 772–777
33. Farlik, M., Rapp, B., Marie, I., Levy, D. E., Jamieson, A. M., and Decker, T. (2012) Contribution of a TANK-binding kinase 1-interferon (IFN) regulatory factor 7 pathway to IFN-γ-induced gene expression. *Mol. Cell Biol.* **32,** 1032–1043
34. Vougioukalaki, M., Kanellis, D. C., Gkouskou, K., and Eliopoulos, A. G. (2011) Tpl2 kinase signal transduction in inflammation and cancer. *Cancer Lett.* **304,** 80–89
35. Beinke, S., Deka, J., Lang, V., Belich, M. P., Walker, P. A., Howell, S., Smerdon, S. J., Gamblin, S. J., and Ley, S. C. (2003) NF-κB1 p105 negatively regulates TPL-2 MEK kinase activity. *Mol. Cell Biol.* **23,** 4739–4752
36. Waterfield, M. R., Zhang, M., Norman, L. P., and Sun, S. C. (2003) NF-κB1/p105 regulates lipopolysaccharide-stimulated MAP kinase signaling by governing the stability and function of the Tpl2 kinase. *Mol. Cell* **11,** 685–694
37. Das, S., Cho, J., Lambertz, I., Kelliher, M. A., Eliopoulos, A. G., Du, K., and Tsichlis, P. N. (2005) Tpl2/cot signals activate ERK, JNK, and NF-κB in a cell-type and stimulus-specific manner. *J. Biol. Chem.* **280,** 23748–23757
38. Eliopoulos, A. G., Wang, C. C., Dumitru, C. D., and Tsichlis, P. N. (2003) Tpl2 transduces CD40 and TNF signals that activate ERK and regulates IgE induction by CD40. *EMBO J.* **22,** 3855–3864
39. Dumitru, C. D., Ceci, J. D., Tsatsanis, C., Kontoyiannis, D., Stamatakis, K., Lin, J. H., Patriotis, C., Jenkins, N. A., Copeland, N. G., Kollias, G., and Tsichlis, P. N. (2000) TNF-α induction by LPS is regulated posttranscriptionally via a Tpl2/ERK-dependent pathway. *Cell* **103,** 1071–1083
40. Eliopoulos, A. G., Dumitru, C. D., Wang, C. C., Cho, J., and Tsichlis, P. N. (2002) Induction of COX-2 by LPS in macrophages is regulated by Tpl2-dependent CREB activation signals. *EMBO J.* **21,** 4831–4840
41. Chiariello, M., Marinissen, M. J., and Gutkind, J. S. (2000) Multiple mitogen-activated protein kinase signaling pathways connect the cot oncoprotein to the c-jun promoter and to cellular transformation. *Mol. Cell Biol.* **20,** 1747–1758
42. Salmeron, A., Ahmad, T. B., Carlile, G. W., Pappin, D., Narsimhan, R. P., and Ley, S. C. (1996) Activation of MEK-1 and SEK-1 by Tpl-2 proto-oncoprotein, a novel MAP kinase kinase kinase. *EMBO J.* **15,** 817–826
43. Tsatsanis, C., Patriotis, C., Bear, S. E., and Tsichlis, P. N. (1998) The Tpl-2 protooncoprotein activates the nuclear factor of activated T cells and induces interleukin 2 expression in T cell lines. *Proc. Natl. Acad. Sci. U.S.A.* **95,** 3827–3832
44. Xiao, N., Eidenschenk, C., Krebs, P., Brandl, K., Blasius, A. L., Xia, Y., Khovananth, K., Smart, N. G., and Beutler, B. (2009) The Tpl2 mutation Sluggish impairs type I IFN production and increases susceptibility to group B streptococcal disease. *J. Immunol.* **183,** 7975–7983
45. Mielke, L. A., Elkins, K. L., Wei, L., Starr, R., Tsichlis, P. N., O'Shea, J. J., and Watford, W. T. (2009) Tumor progression locus 2 (Map3k8) is critical for host defense against *Listeria* monocytogenes and IL-1β production. *J. Immunol.* **183,** 7984–7993
46. Kaiser, F., Cook, D., Papoutsopoulou, S., Rajsbaum, R., Wu, X., Yang, H. T., Grant, S., Ricciardi-Castagnoli, P., Tsichlis, P. N., Ley, S. C., and O'Garra, A. (2009) TPL-2 negatively regulates interferon-β production in macrophages and myeloid dendritic cells. *J. Exp. Med.* **206,** 1863–1871
47. Yang, H. T., Wang, Y., Zhao, X., Demissie, E., Papoutsopoulou, S., Mambole, A., O'Garra, A., Tomczak, M. F., Erdman, S. E., Fox, J. G., Ley, S. C., and Horwitz, B. H. (2011) NF-κB1 inhibits TLR-induced IFN-β production in macrophages through TPL-2-dependent ERK activation. *J. Immunol.* **186,** 1989–1996
48. Watford, W. T., Hissong, B. D., Durant, L. R., Yamane, H., Muul, L. M., Kanno, Y., Tato, C. M., Ramos, H. L., Berger, A. E., Mielke, L., Pesu, M., Solomon, B., Frucht, D. M., Paul, W. E., Sher, A., Jankovic, D., Tsichlis, P. N., and O'Shea, J. J. (2008) Tpl2 kinase regulates T cell interferon-γ production and host resistance to *Toxoplasma gondii*. *J. Exp. Med.* **205,** 2803–2812
49. Stojdl, D. F., Lichty, B. D., tenOever, B. R., Paterson, J. M., Power, A. T., Knowles, S., Marius, R., Reynard, J., Poliquin, L., Atkins, H., Brown, E. G., Durbin, R. K., Durbin, J. E., Hiscott, J., and Bell, J. C. (2003) VSV strains with defects in their ability to shutdown innate immunity are potent sys-

temic anti-cancer agents. *Cancer Cell* **4,** 263–275
50. Donelan, N. R., Basler, C. F., and García-Sastre, A. (2003) A recombinant influenza A virus expressing an RNA-binding-defective NS1 protein induces high levels of β interferon and is attenuated in mice. *J. Virol.* **77,** 13257–13266
51. Sharma, S., tenOever, B. R., Grandvaux, N., Zhou, G. P., Lin, R., and Hiscott, J. (2003) Triggering the interferon antiviral response through an IKK-related pathway. *Science* **300,** 1148–1151
52. Mibayashi, M., Martínez-Sobrido, L., Loo, Y. M., Cárdenas, W. B., Gale, M., Jr., and García-Sastre, A. (2007) Inhibition of retinoic acid-inducible gene I-mediated induction of β interferon by the NS1 protein of influenza A virus. *J. Virol.* **81,** 514–524
53. Niwa, H., Yamamura, K., and Miyazaki, J. (1991) Efficient selection for high-expression transfectants with a novel eukaryotic vector. *Gene* **108,** 193–199
54. Newhart, A., Negorev, D. G., Rafalska-Metcalf, I. U., Yang, T., Maul, G. G., and Janicki, S. M. (2013) Sp100A promotes chromatin decondensation at a cytomegalovirus-promoter-regulated transcription site. *Mol. Biol. Cell* **24,** 1454–1468
55. tenOever, B. R., Ng, S. L., Chua, M. A., McWhirter, S. M., García-Sastre, A., and Maniatis, T. (2007) Multiple functions of the IKK-related kinase IKKε in interferon-mediated antiviral immunity. *Science* **315,** 1274–1278
56. Perez, J. T., Varble, A., Sachidanandam, R., Zlatev, I., Manoharan, M., García-Sastre, A., and tenOever, B. R. (2010) Influenza A virus-generated small RNAs regulate the switch from transcription to replication. *Proc. Natl. Acad. Sci. U.S.A.* **107,** 11525–11530
57. Varble, A., Benitez, A. A., Schmid, S., Sachs, D., Shim, J. V., Rodriguez-Barrueco, R., Panis, M., Crumiller, M., Silva, J. M., Sachidanandam, R., and Tenoever, B. R. (2013) An *in vivo* RNAi screening approach to identify host determinants of virus replication. *Cell Host Microbe* **14,** 346–356
58. Levy, D. E., Kessler, D. S., Pine, R., Reich, N., and Darnell, J. E., Jr. (1988) Interferon-induced nuclear factors that bind a shared promoter element correlate with positive and negative transcriptional control. *Genes Dev.* **2,** 383–393
59. Fitzgerald, K. A., McWhirter, S. M., Faia, K. L., Rowe, D. C., Latz, E., Golenbock, D. T., Coyle, A. J., Liao, S. M., and Maniatis, T. (2003) IKKε and TBK1 are essential components of the IRF3 signaling pathway. *Nat. Immunol.* **4,** 491–496
60. Qin, B. Y., Liu, C., Lam, S. S., Srinath, H., Delston, R., Correia, J. J., Derynck, R., and Lin, K. (2003) Crystal structure of IRF-3 reveals mechanism of autoinhibition and virus-induced phosphoactivation. *Nat. Struct. Biol.* **10,** 913–921
61. Takahasi, K., Suzuki, N. N., Horiuchi, M., Mori, M., Suhara, W., Okabe, Y., Fukuhara, Y., Terasawa, H., Akira, S., Fujita, T., and Inagaki, F. (2003) X-ray crystal structure of IRF-3 and its functional implications. *Nat. Struct. Biol.* **10,** 922–927
62. Yang, H., Lin, C. H., Ma, G., Orr, M., Baffi, M. O., and Wathelet, M. G. (2002) Transcriptional activity of interferon regulatory factor (IRF)-3 depends on multiple protein-protein interactions. *Eur. J. Biochem.* **269,** 6142–6151
63. Lin, R., Mamane, Y., and Hiscott, J. (2000) Multiple regulatory domains control IRF-7 activity in response to virus infection. *J. Biol. Chem.* **275,** 34320–34327
64. Wathelet, M. G., Lin, C. H., Parekh, B. S., Ronco, L. V., Howley, P. M., and Maniatis, T. (1998) Virus infection induces the assembly of coordinately activated transcription factors on the IFN-β enhancer *in vivo*. *Mol. Cell* **1,** 507–518
65. Rand, U., Rinas, M., Schwerk, J., Nöhren, G., Linnes, M., Kröger, A., Flossdorf, M., Kály-Kullai, K., Hauser, H., Höfer, T., and Köster, M. (2012) Multi-layered stochasticity and paracrine signal propagation shape the type-I interferon response. *Mol. Syst. Biol.* **8,** 584
66. Servant, M. J., Grandvaux, N., tenOever, B. R., Duguay, D., Lin, R., and Hiscott, J. (2003) Identification of the minimal phosphoacceptor site required for *in vivo* activation of interferon regulatory factor 3 in response to virus and double-stranded RNA. *J. Biol. Chem.* **278,** 9441–9447
67. Wang, J. T., Doong, S. L., Teng, S. C., Lee, C. P., Tsai, C. H., and Chen, M. R. (2009) Epstein-Barr virus BGLF4 kinase suppresses the interferon regulatory factor 3 signaling pathway. *J. Virol.* **83,** 1856–1869
68. Au, W. C., Yeow, W. S., and Pitha, P. M. (2001) Analysis of functional domains of interferon regulatory factor 7 and its association with IRF-3. *Virology* **280,** 273–282
69. Chen, W., Lam, S. S., Srinath, H., Jiang, Z., Correia, J. J., Schiffer, C. A., Fitzgerald, K. A., Lin, K., and Royer, W. E., Jr. (2008) Insights into interferon regulatory factor activation from the crystal structure of dimeric IRF5. *Nat. Struct. Mol. Biol.* **15,** 1213–1220
70. Borden, K. L. (2008) Pondering the puzzle of PML (promyelocytic leukemia) nuclear bodies. Can we fit the pieces together using an RNA regulon? *Biochim. Biophys. Acta* **1783,** 2145–2154
71. Geoffroy, M. C., and Chelbi-Alix, M. K. (2011) Role of promyelocytic leukemia protein in host antiviral defense. *J. Interferon Cytokine Res.* **31,** 145–158
72. Lallemand-Breitenbach, V., and de Thé, H. (2010) PML nuclear bodies. *Cold Spring Harb. Perspect. Biol.* **2,** a000661
73. Grötzinger, T., Jensen, K., and Will, H. (1996) The interferon (IFN)-stimulated gene Sp100 promoter contains an IFN-γ activation site and an imperfect IFN-stimulated response element which mediate type I IFN inducibility. *J. Biol. Chem.* **271,** 25253–25260
74. Doody, G. M., Care, M. A., Burgoyne, N. J., Bradford, J. R., Bota, M., Bonifer, C., Westhead, D. R., and Tooze, R. M. (2010) An extended set of PRDM1/BLIMP1 target genes links binding motif type to dynamic repression. *Nucleic Acids Res.* **38,** 5336–5350
75. Wang, J., Shiels, C., Sasieni, P., Wu, P. J., Islam, S. A., Freemont, P. S., and Sheer, D. (2004) Promyelocytic leukemia nuclear bodies associate with transcriptionally active genomic regions. *J. Cell Biol.* **164,** 515–526
76. Seth, R. B., Sun, L., Ea, C. K., and Chen, Z. J. (2005) Identification and characterization of MAVS, a mitochondrial antiviral signaling protein that activates NF-κB and IRF 3. *Cell* **122,** 669–682
77. Fensterl, V., and Sen, G. C. (2009) Interferons and viral infections. *Biofactors* **35,** 14–20
78. Thakar, J., Schmid, S., Duke, J. L., Garcia-Sastre, A., and Kleinstein, S. H. (2013) Overcoming NS1-mediated immune antagonism involves both interferon-dependent and independent mechanisms. *J. Interferon Cytokine Res.* **33,** 700–708
79. Baum, A., Sachidanandam, R., and García-Sastre, A. (2010) Preference of RIG-I for short viral RNA molecules in infected cells revealed by next-generation sequencing. *Proc. Natl. Acad. Sci. U.S.A.* **107,** 16303–16308
80. Langlois, R. A., Varble, A., Chua, M. A., García-Sastre, A., and tenOever, B. R. (2012) Hematopoietic-specific targeting of influenza A virus reveals replication requirements for induction of antiviral immune responses. *Proc. Natl. Acad. Sci. U.S.A.* **109,** 12117–12122
81. Rehwinkel, J., Tan, C. P., Goubau, D., Schulz, O., Pichlmair, A., Bier, K., Robb, N., Vreede, F., Barclay, W., Fodor, E., and Reis e Sousa, C. (2010) RIG-I detects viral genomic RNA during negative-strand RNA virus infection. *Cell* **140,** 397–408
82. Moltedo, B., Li, W., Yount, J. S., and Moran, T. M. (2011) Unique type I interferon responses determine the functional fate of migratory lung dendritic cells during influenza virus infection. *PLoS Pathog.* **7,** e1002345
83. Kumar, P. P., Bischof, O., Purbey, P. K., Notani, D., Urlaub, H., Dejean, A., and Galande, S. (2007) Functional interaction between PML and SATB1 regulates chromatin-loop architecture and transcription of the MHC class I locus. *Nat. Cell Biol.* **9,** 45–56
84. Ulbricht, T., Alzrigat, M., Horch, A., Reuter, N., von Mikecz, A., Steimle, V., Schmitt, E., Krämer, O. H., Stamminger, T., and Hemmerich, P. (2012) PML promotes MHC class II gene expression by stabilizing the class II transactivator. *J. Cell Biol.* **199,** 49–63
85. Hayakawa, F., and Privalsky, M. L. (2004) Phosphorylation of PML by mitogen-activated protein kinases plays a key role in arsenic trioxide-mediated apoptosis. *Cancer Cell* **5,** 389–401
86. Bonilla, W. V., Pinschewer, D. D., Klenerman, P., Rousson, V., Gaboli, M., Pandolfi, P. P., Zinkernagel, R. M., Salvato, M. S., and Hengartner, H. (2002) Effects of promyelocytic leukemia protein on virus-host balance. *J. Virol.* **76,** 3810–3818
87. Blondel, D., Kheddache, S., Lahaye, X., Dianoux, L., and Chelbi-Alix, M. K. (2010) Resistance to rabies virus infection conferred by the PMLIV isoform. *J. Virol.* **84,** 10719–10726
88. Iki, S., Yokota, S., Okabayashi, T., Yokosawa, N., Nagata, K., and Fujii, N.

(2005) Serum-dependent expression of promyelocytic leukemia protein suppresses propagation of influenza virus. *Virology* **343,** 106–115
89. Chelbi-Alix, M. K., Quignon, F., Pelicano, L., Koken, M. H., and de Thé, H. (1998) Resistance to virus infection conferred by the interferon-induced promyelocytic leukemia protein. *J. Virol.* **72,** 1043–1051
90. Tavalai, N., and Stamminger, T. (2008) New insights into the role of the subnuclear structure ND10 for viral infection. *Biochim. Biophys. Acta* **1783,** 2207–2221
91. Xu, J., Hopkins, K., Sabin, L., Yasunaga, A., Subramanian, H., Lamborn, I., Gordesky-Gold, B., and Cherry, S. (2013) ERK signaling couples nutrient status to antiviral defense in the insect gut. *Proc. Natl. Acad. Sci. U.S.A.* **110,** 15025–15030